

Fin Flutter Analysis

Richard Bauer and Austin Hardman

California Polytechnic State University: San Luis Obispo, San Luis Obispo, California, 93401

This report summarizes the experimental process executed to study fin flutter characteristics. The experiment analyzed the influence of the relationship between structural dynamics and aerodynamics on flutter characteristics. Theoretical models were created in PATRAN/NASTRAN and FinSim for comparison to experimental results and to set the envelope of the physical experiments. The theoretical analysis predicted the occurrence of flutter near Mach 1 or Mach 5. The physical model was constructed of solid aluminum with machined holes for the inertial sensors. Two test runs were completed to collect data on the displacement of the fin in the supersonic wind tunnel. Additionally, the tests sought to identify any evidence of flutter as determined by the theorized model. The results showed evidence of both bending and twisting in the fin.

Nomenclature

A	=	area of the test section
A^*	=	throat area
M	=	Mach number
P	=	pressure
P_0	=	static pressure
γ	=	specific heat ratio

Contents

Fin Flutter Senior Project.....	1
I. Introduction.....	3
II. Airfoil and Wing Selection.....	3
III. Theoretical Analysis.....	4
IV. Experimental Testing.....	6
A. Accelerometer Throughput Test.....	6
B. Accelerometer Locations.....	9
C. Experiment Set-up.....	10
D. Procedure.....	11
E. Tunnel Mach Number.....	12
V. Results.....	13
A. SSWT Testing.....	13
B. Displacement Visualizations.....	16
VI. Future Work.....	18
VII. Conclusion.....	20
References.....	21

Figures

Figure 1. Wing Geometry with Applied Root Boundary Conditions.....	5
Figure 2. Displacement Results of the First Normal Mode.....	6
Figure 3. Accelerometer Throughput Test.....	8
Figure 4. Selection of Calibration.....	9
Figure 5. Experiment Model.....	10
Figure 6. Accelerometer Locations.....	10
Figure 7. Fin in the Test Section.....	11
Figure 8. Quick Disconnect Interface.....	11
Figure 9. DAQ Wiring.....	11
Figure 10. SSWT Run Number 1.....	13
Figure 11. SSWT Run Number 2.....	13
Figure 12. Relative Displacement Run 1.....	14
Figure 13. Relative Displacement Run 2.....	15
Figure 14. Fin Displacement Over Time.....	17
Figure 15. Image of the Fin After Run 2.....	18
Figure 16. Highlighted portion of Figure 16.....	18
Figure 17. Detached Accelerometers.....	19

Tables

Table 1. Frequency Values for the Structural Normal Modes.....	5
Table 2. USB DAQ Characteristics.....	7
Table 3. Accelerometer Characteristics.....	7
Table 4. Area Ratio Equation Numbers to Solve for Mach Number.....	12

I. Introduction

Flying structures demand light materials capable of withstanding strong aerodynamic loads present during flight. Aeroelasticity is the interaction of inertial, aerodynamic, and elastic forces of flight vehicles.¹ Flutter is an aeroelastic instability commonly seen in wings, tails, rotor blades and control surfaces of aircraft, as well as rocket fins. The phenomenon occurs when aerodynamic loads cause deformation of the body, which in turn creates a reaction by the structure, initiating an oscillatory motion. Under deformation, the aerodynamics of the wing change, which results in the body absorbing energy from the airflow and the amplitudes of the oscillations may increase to the level of fracture or instability.

Although all flutter follows the basic pattern of inertial, aerodynamic, and elastic interaction, the exact causes and effects may vary. There are several types of flutter for aircraft and variations specific to rockets and missiles. Aircraft may experience panel flutter, galloping flutter, stall flutter, limit cycle oscillations (LCO), and propeller whirl flutter. Examples of flutter problems for missiles include skin flutter, flutter of automatic controls or servomechanics, and flutter of short wings with ram-jets or external stores.²

The type of flutter being investigated in this work is wing bending-torsion flutter. Aerodynamic fluctuations of the supersonic region create an inertial offset in the wing. The structural responses of the wing have a phase difference between bending and torsion, preventing the reactions from dampening each other out.³ Flutter velocity is the airspeed where the structure oscillates in an unstable harmonic motion. Cal Poly's supersonic wind tunnel was utilized to validate the flutter velocity from modeling in PATRAN and FinSim analyses.

Flutter testing has become an integral part of the design process to ensure survivability. This project aims to develop the basis of an investigation of the phenomenon and encourages future exploration. Flutter can cause vehicle structures to fail, and is an important element of the flight envelope to investigate.

II. Airfoil and Wing Selection

Contrary to standard aircraft, the experimental wing used in this work needed to be designed to flutter. Research was completed to identify wings previously shown to flutter and alterations that affect flutter velocity, such as sweep and camber. The initial choice was the F-16 wing due to its historical

connection with flutter characteristics. However, further investigation revealed the flutter instability occurs in the wing due to hanging loads, especially the wingtip Sidewinder. The F-16 wing was not chosen due to the complexity and safety risks of creating a wing with detachable pieces for the supersonic wind tunnel tests. Further research provided a wing proven to flutter without additions to the basic geometry.

A NASA research video documented flutter tests for the X-15 horizontal stabilator. The video illustrated the potential for the stabilator to flutter during wind tunnel testing. The airfoil on the X-15 was a customized model and the coordinates were unobtainable for modeling. Similar airfoils were plotted on top of an image of the original NACA 66005 in order to choose a new geometry. The sweep and lack of camber present in the X-15 stabilator favorably reduced the flutter velocity towards the regime predicted for the supersonic wind tunnel. Airfoil coordinate data was selected from the UICI database for the NACA 66206 airfoil.

The model was further modified for manufacturing constraints and integration of the sensors. The root thickness was increased for the two AN-632 bolts used to fasten the wing to the test stand. Similarly, the wingtip thickness was expanded to contain the MMA2301KEG-ND accelerometers. Therefore, the final wing has a NACA 66212 for the root and a NACA 66215 at the wingtip.

III. Theoretical Analysis

NASTRAN and PATRAN were the primary finite element analysis (FEA) software used in the theoretical development of the wing. Additionally, FinSim was used for confirmation of results and identification of the required flutter velocity. PATRAN is a program that allows the user to analyze a geometry created internally or imported from outside programs, such as SolidWorks. The analysis tools include the ability to set boundary conditions, initial and final load sets, material properties, aerodynamic forces and properties. NASTRAN is an FEA program that takes the data produced by PATRAN and solves for the desired outputs. For this experiment, the desired outputs were the normal modes of the wing as well as the flutter speed. For the purposes of this experiment, a 2-D model was used with similar geometric characteristics related to the X-15 horizontal stabilator. Figure 1 shows the 3-D model created in PATRAN with the boundary conditions applied. The AN-632 bolts are represented as rigid connection boundary conditions, while the rest of the model represents a semi-rigid connection. The semi-rigid connection prevents linear movement in all directions, but allows for bending and torsional flexing.

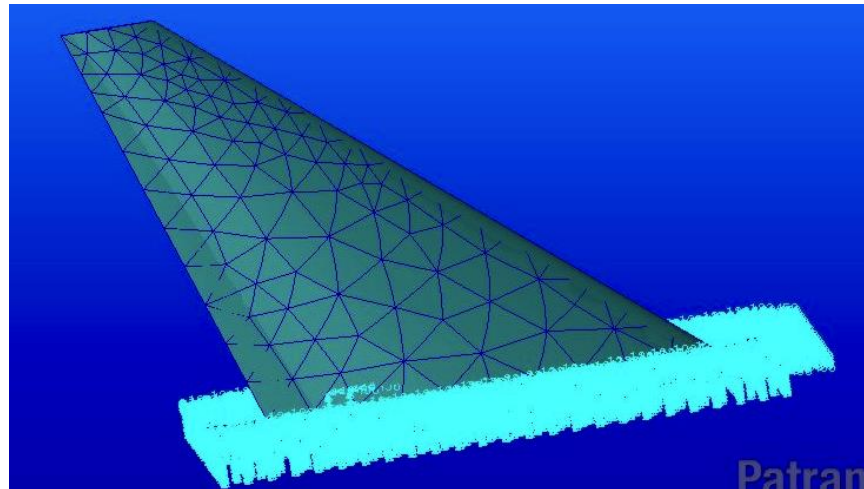


Figure 1. Wing Geometry with Applied Root Boundary Conditions.

The first step in the analysis process was to calculate the structural nodes, which was completed using NASTRAN. After setting the boundary conditions on the model, as shown in Figure 1, the NASTRAN analysis solution was set to normal modes in order to analyze the structure to calculate its normal modes. Table 1 shows the values for the frequencies where the normal modes occur.

Table 1. Frequency Values for the Structural Normal Modes.

Normal Mode	Frequency
Mode 1	1189 Hz
Mode 2	3390 Hz
Mode 3	5522 Hz

Although the results do seem high, it was assumed that the material being used was made out of aluminum, which at the time of the analysis sufficed. Changing the material to be more ductile will drastically reduce these numbers. Note that these numbers are the normal modes of the structure, and not necessarily the frequency at which the structure will flutter. Although PATRAN/NASTRAN has the capability to do aero-elastic analysis, the analysis was not able to be done in the allotted time. The flutter software, FinSim, was used in conjunction with the NASTRAN findings. It confirmed the normal modes of the structure as well as produced an estimation of the divergence velocity and flutter frequency.

The next step component was the displacement that was caused by the normal modes. This was important to calculate since if the displacement was high enough to fracture the fin, then a different material had to be chosen. As stated previously, the chosen material was aluminum, which has an average

ductile material property. Once again, changing the material to be more ductile will drastically increase the deflection of the fin.

The original goal of the project was to create an FEA model and subject it to an aeroelastic analysis in PATRAN in order to figure out the divergence velocity, as well as determine the frequency in which the fin would flutter. The normal modes of the fin were discovered using the software. Although this validation was not able to be completed, the model could be verified by placing the fin on a shake table to match the normal modes produced by PATRAN. Figure 2 shows the results of the first normal mode. The units are in inches; however, there is a scaling factor of 0.1 that is not shown in the figure. This scaling factor means that the actual displacement of the fin would be closer to 0.986 inches and not the 9.86 result that is currently shown.

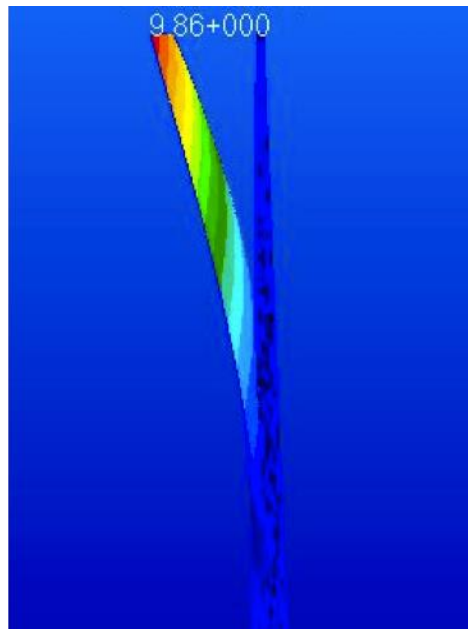


Figure 2. Displacement Results of the First Normal Mode.

IV. Experimental Testing

A. Accelerometer Throughput Test

To measure the displacement of the fin while it was running in the tunnel, 1-D accelerometers were connected to four distinct points on the fin. The accelerometers needed to have a high sample rate due to the high frequency in which the fin was expected to vibrate. Furthermore, the accelerometers needed to survive the supersonic environment. Performance compromises were made in selecting the

MMA2301KEG-ND accelerometer. Other accelerometers with higher performance capabilities were purchased and tested for use in the experiment. Several factors eliminated the other accelerometer options. For example, the Analog Device ADXL326 3-D sensor was desired for its small size (4 x 4 mm), increased sensitivity (~60 mV/g), and faster sample rate (550 samples/sec). However, it was eliminated because the team could not securely solder the wire leads, breaking the connections through handling the wired accelerometer alone.

A National Instruments Data Acquisition (DAQ) module was used for the testing purposes. The key specifications of the DAQ are shown in Table 2. The DAQ was selected due to its high accuracy and rather high sample rate. Furthermore, the DAQ is available in the Cal Poly laboratories and the team is familiar with its use from previous laboratory experiments. A Freescale Semiconductor Low G Micromachined Accelerometer was also used for testing. The specific model is the MMA2301KEG-ND accelerometer from Digikey. Its key specifications are shown in Table 3.

Table 2. USB DAQ Characteristics. *Operating limitations of the DAQ.*

Component	A-D Resolution	Sample Rate	Min Voltage Range Accuracy	Max Voltage Range Accuracy
NI USB-6211 Data Acquisition Module	16-bit	250kS/s	0.088mV	2.69 mV

Table 3. Accelerometer Characteristics. *Operating limitations of the accelerometers.*

Component	Operating Characteristics				
		Min	Typical	Max	Units
FS MMA2301KEG-ND Accelerometer	Sensitivity	693.8	750	806.3	mV/g
	Operating Voltage	4.75	5	5.25	V
	Acceleration Limits	-2.5	--	2.5	g

The accelerometers were tested before being included in the experiment. The throughput test increased the team's familiarity with the accelerometers and allowed for the successful setup of the LabView software. Figure 3 shows the data for the entire calibration test. Figure 4 is zoomed in section of the previous figure. During the test, the accelerometers were mounted to a stationary platform and hooked

onto a spring mechanism. The spring was displaced and the platform oscillated up and down. Figure 3 displays the entire test data. Instances of the platform being held stationary can be seen, as well as time periods where the platform moved on the spring mechanism. Figure 4 highlights an oscillatory motion section from the accelerometer calibration. The throughput test showed that the sample frequency was also affected by the LabView software. Despite the hardware specifications listing high sample rates for the accelerometers and DAQ module, the bottleneck seemed to be LabView, which decreased the data collection rate down to 36 samples per second.

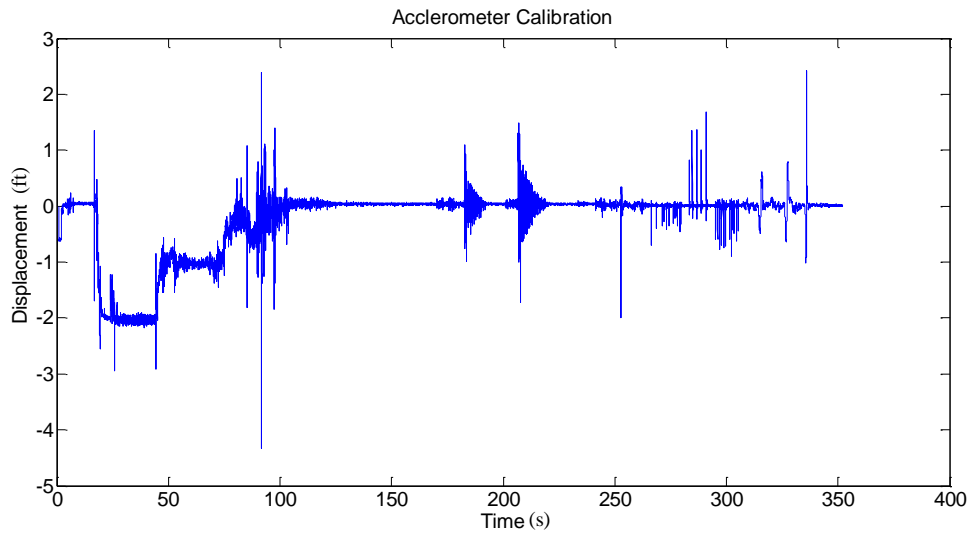


Figure 3. Accelerometer Throughput Test. *The accelerometers and the LabView software underwent a throughput test before entry into the wind tunnel. In this test, the accelerometer was placed on a spring mechanism and allowed to oscillate. Additionally, the mechanism was tapped with a hammer to create very short period vibrations.*

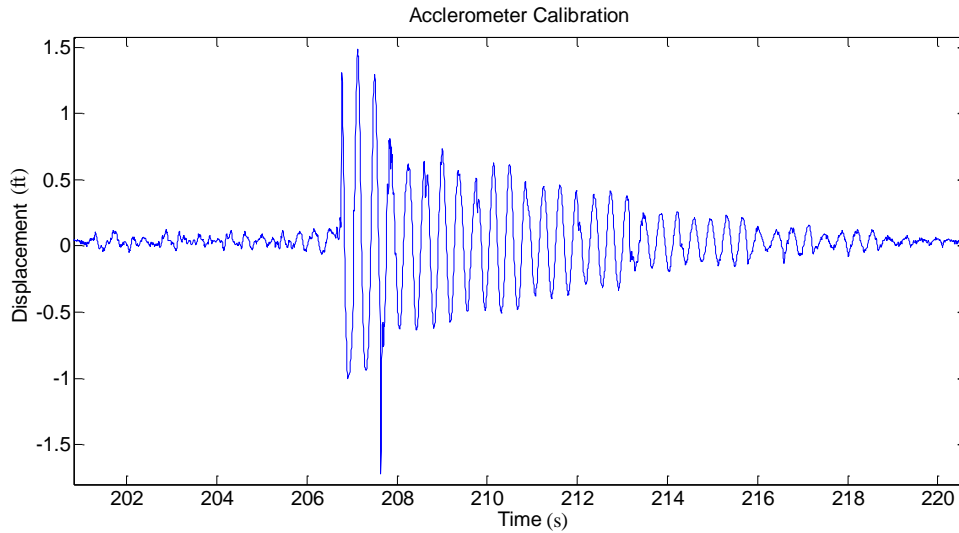


Figure 4. Selection of Calibration. *This section of data highlights an oscillatory motion section of the accelerometer calibration.*

B. Accelerometer Locations

The Cal Poly Supersonic Wind Tunnel (SSWT) was used for experimental testing. The fin was theoretically calculated using FinSim to flutter in the transonic region and at approximately Mach 5. However, the supersonic wind tunnel was configured to achieve an airflow speed of approximately Mach 3.3. The difference between the ideal test speed and the test conditions was an area of concern going into the test. Accelerometers were used to collect acceleration data on the fin's movement and placed in four distinct locations on the fin. Accelerometer one was located at the very top, where the displacement from the flutter was predicted to be the largest magnitude. Two accelerometers were placed towards the middle along the same chord line. The overall translational displacement was expected to be the same, but differences in movement were indicative of torsional displacement. The fourth accelerometer was placed near the root as a reference for noise in the data. Figure 5 shows how the accelerometers were mounted in the actual fin. Figure 6 shows the layout of the accelerometers and their respective numbers.



Figure 5. Experiment Model. *View of the actual model wing.*

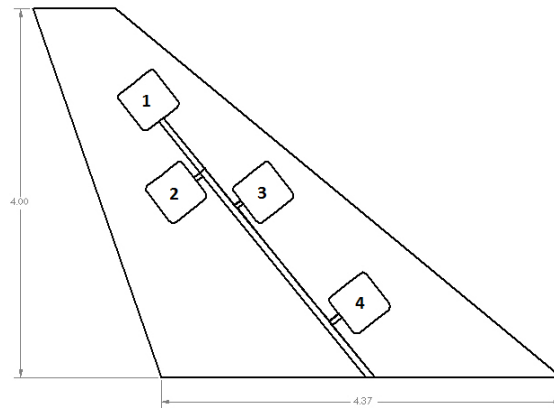


Figure 6. Accelerometer Locations. *Locations of the accelerometers in the fin.*

A channel was created in the middle of the fin to feed the wires through. A total of 12 wires ran through the fin. Each accelerometer required one wire for the input voltage, the output voltage, and the ground. The output voltage is the signal and converted in the LabView software to acceleration.

C. Experiment Set-up

The three wires (signal, power, and ground) were soldered to the accelerometers. Next, the accelerometers were secured in the fin using Mortite caulking putty. The putty was non-conductive and could be smoothed over the accelerometer to match the original airfoil's shape. The wires were fed through the central channel and out through a hole in the center of the fixture plate. The fixture plate was attached to the top of the SSWT test section, securing the fin in place, as shown in Figure 7.



Figure 7. Fin in the Test Section. *A view of the fin in the test section from behind the trailing edge.*

External to the test section, the wires were attached to shielded cabling. The connection was made using a quick disconnect interface. The shielded wires were then connected to a DAQ located in the control room. The DAQ was then connected to a computer, also located in the control room. Figure 8 shows the quick disconnect used as the interface between the wires coming from the fin and the shielded wires that went from the interface to the DAQ. Figure 9 shows the wiring of the DAQ used for the experiment.

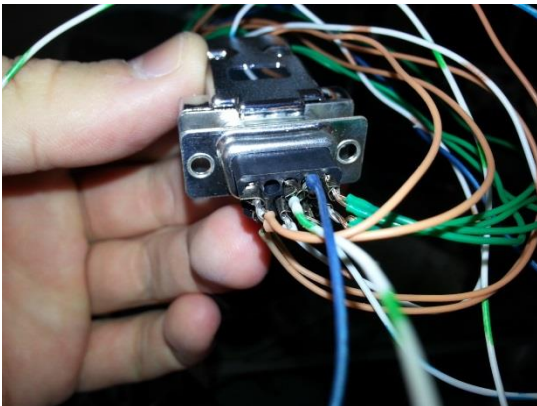


Figure 8. Quick Disconnect Interface. *The connection between the accelerometer wires and the shielded cable.*



Figure 9. DAQ Wiring. *The wiring from the shielded cable to the DAQ.*

D. Procedure

The test procedure followed closely to that of the supersonic wind tunnel operation safety plan. All of the necessary safety precautions were taken prior to running the tunnel. When the pre-run checklist

was complete, the manual valve of the tunnel was opened. The software operator in the control room initiated the collection of data through LabView. Next, the electro-pneumatic valve was opened via an electronic switch inside the control room, removing the final seal and allowing the tank pressure to push through the wind tunnel. After approximately 10 seconds, the electro-pneumatic valve was closed again, via the switch in the control room. This stopped the airflow into the tunnel. The software operator stopped the program and saved the data file. After it was confirmed that the tunnel was off, the manual valve was closed. The post-run checklist was then completed to ensure that the tunnel was shut off correctly, and that it was safe to work around.

E. Tunnel Mach Number

In order to determine at what speed the fin fluttered the most, it was necessary to figure out the Mach number in the test section throughout the course of the test run. Normally, pressure transducers are placed upstream and downstream of the wind tunnel, and the pressure ratio between the two is used to calculate the Mach number. From there the pressure ratio Mach number equation can be used to find the resulting Mach number. However, due to the oblique shocks coming off of the fin that were hitting the downstream pitot tube, the resulting pressure readings were incorrect for calculating the tunnel's airspeed. Thus, the area ratio Mach number equation was used. The area ratio equation is based on the areas of the test section and throat and is not affected by the oblique shocks coming from the fin. Equation 1 shows the pressure ratio equation and Equation 2 shows the area ratio equation. Table 4 shows the various numbers used to calculate the Mach number, as well as the calculated Mach number affecting the fin.

$$\frac{P}{P_o} = \left(1 + \frac{\gamma - 1}{2} M^2\right)^{\frac{-\gamma}{\gamma - 1}} \quad (1)$$

$$\frac{A}{A^*} = \frac{(\gamma + 1)^{\frac{-(\gamma + 1)}{2(\gamma - 1)}}}{2} \frac{\left(1 + \frac{(\gamma - 1)}{2} M^2\right)^{\frac{(\gamma + 1)}{2(\gamma - 1)}}}{M} \quad (2)$$

Table 4. Area Ratio Equation Numbers to Solve for Mach Number.

Test Section Area	Throat Area	Specific Heat Ratio	Mach Number
23.6 in ²	4.18 in ²	1.4	3.31

V. Results

A. SSWT Testing

In order to validate the analytical predictions mentioned above, several tests were run in the aforementioned Cal Poly Supersonic Wind Tunnel. Acceleration data was collected and integrated into position data. The results of the two experimental SSWT runs are shown below in Figure 10 and Figure 11. It is important to note that the data is not shown from time equal to zero. As mentioned in the procedure, lag time occurs before the initiation of the data collection and the initiation of the tunnel. Therefore, the figures only display the period of time when the tunnel was operating.

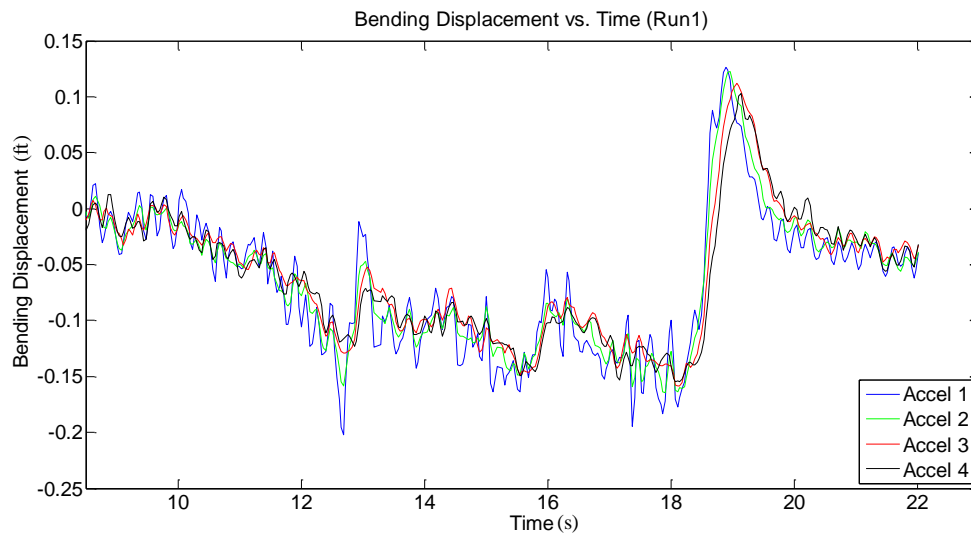


Figure 10. SSWT Run Number 1.

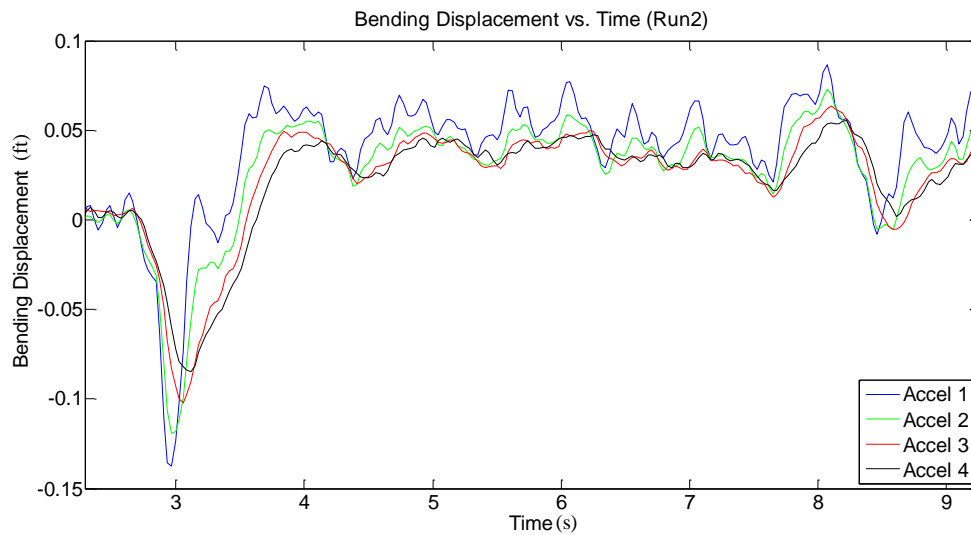


Figure 11. SSWT Run Number 2.

In both experimental runs, an offset position occurred. The data shifts towards an offset value and oscillates around that displacement measurement. Run 1 settled around downward deflection of 0.1 feet. Run 2 settled around an upward deflection of 0.05 feet. This offset did not make physical sense, so steps were taken to eliminate its evidence in the data. Accelerometer four is located near the support bolts in the fin, and little to no movement was projected for this area of the fin. Any movement read by the fourth accelerometer was therefore considered to be noise. The vibration of the tunnel during operation and external electrical interference are two possible causes of noise in the data. Accelerometer four's data was used in post processing as a reference for noise to improve the accuracy of all of the data. Data from accelerometers one, two and three were adjusted to be relative to accelerometer four. This nominalized data output is show in Figure 12 and Figure 13 for Run 1 and Run2, respectively.

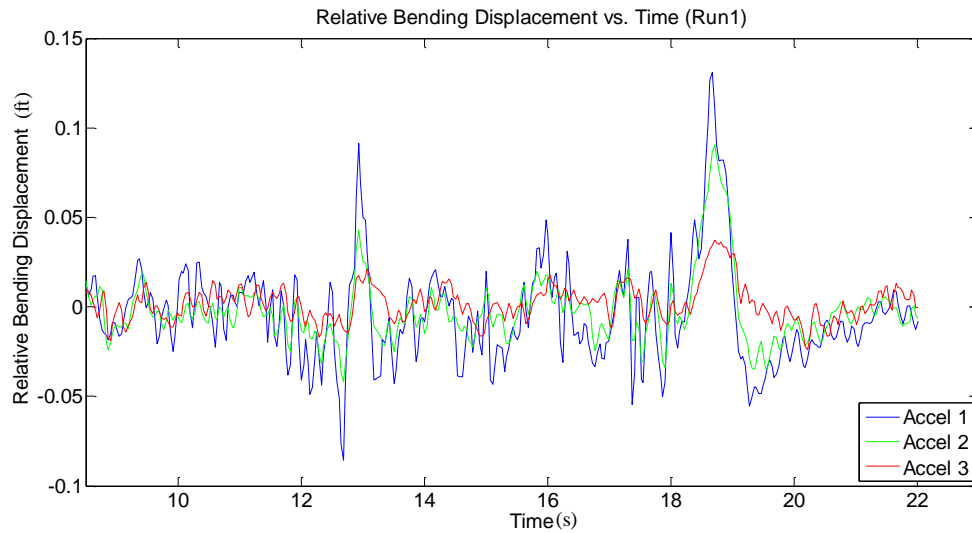


Figure 12. Relative Displacement Run 1.

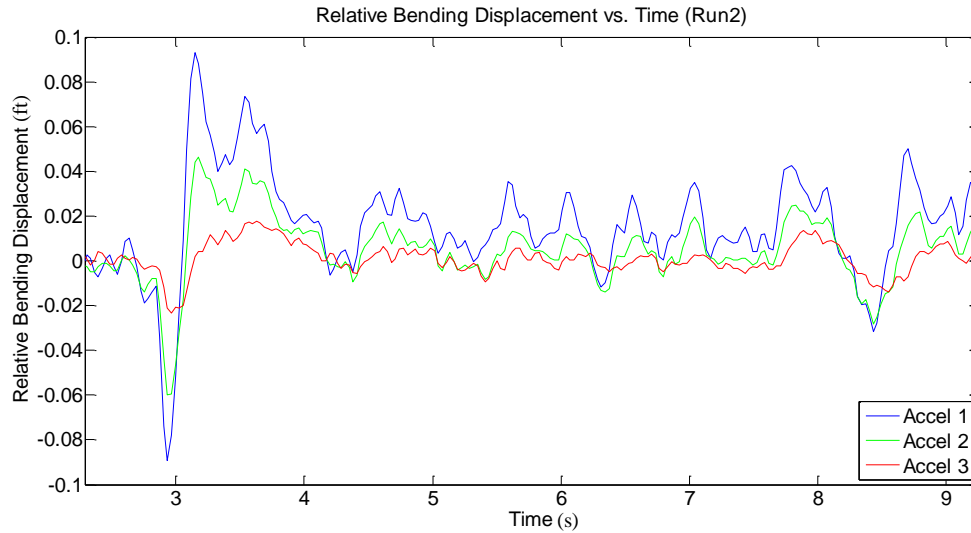


Figure 13. Relative Displacement Run 2.

Several aspects within the plots are important. Accelerometer 1, the wingtip sensor, underwent the greatest deflection in both trials. Accelerometer 2, the aft accelerometer, experienced greater bending than accelerometer 3, indicating twist in the wing. The data is similar to the trend of increased bending that was predicted in the theoretical analysis. This identification also follows basic beam bending theory. However, caution must be taken in considering the results. The sample rate achieved by the data acquisition system is much lower than the predicted frequency of oscillations in the theoretical analysis. Additionally, referencing the data to the fourth accelerometer compounds any possible errors in the data measurements. Improvements for these shortcomings in the data analysis are discussed later in the report.

Bending-torsion flutter is the focus of this experiment. Regarding Figure 13, bending occurs around the 3.5 to 4 second time period after the initial shockwave from the tunnel has passed. In the same time period, accelerometer two moves significantly farther than accelerometer three, indicating torsion. Both the bending and torsion continue in an oscillatory pattern from the 4.5 to 7.5 second time period in the plot, failing to dampen each other out.

All three accelerometers are shown to displace at eight seconds. At this point, the data illustrates a displacement pattern similar to the dynamics of flutter. Once again, caution must be taken when considering this result due to the inaccuracies of the data measurement system. The stiffness of the wing resists the displacement shown at the eight second mark, pulling the wing back towards its neutral position. Assuming the dynamics of flutter were captured accurately, the response bend absorbed additional energy

from the airflow causing the wing to twist, as seen in the 8.5 second mark of Figure 13. The extra energy produces the next wing bend, back towards the positive direction, with a greater tip deflection than the previous positive displacement. Another example of this occurrence is shown in Figure 12 around the 13 second time period.

Assuming the displacements were properly captured, and despite the fin movement dampening out in the next oscillation, this is a brief example of the dangers of fin flutter. Offset bending and torsion responses within the wing, allow for additional energy absorption from the airflow, amplifying the movement of the wing. In true bending-torsion flutter, the offset responses and wing movement would continue, risking damage to the structure and failure of the aircraft.

B. Displacement Visualizations

The large spike in movement, located around three seconds in run number two, has been simulated in Figure 14. The data was animated in a Matlab plot to visualize the movement of the fin. Figure 14 is included below as a representative sample of the animated plot. The period of time in the data is selected due to the large displacement values in order to easily communicate the concept of the animation.

The blue line is representative of the fin based on accelerometers one, three and four, while the red line is representative of the fin utilizing accelerometers one, two and four. Accelerometers two and three are located the same distance along the span, varying in distance along the chord. Differences in the movement between these accelerometers are suggestive of twist occurring in the wing. Therefore, the difference between the red and blue lines is indicative of the amount of twist in the wing.

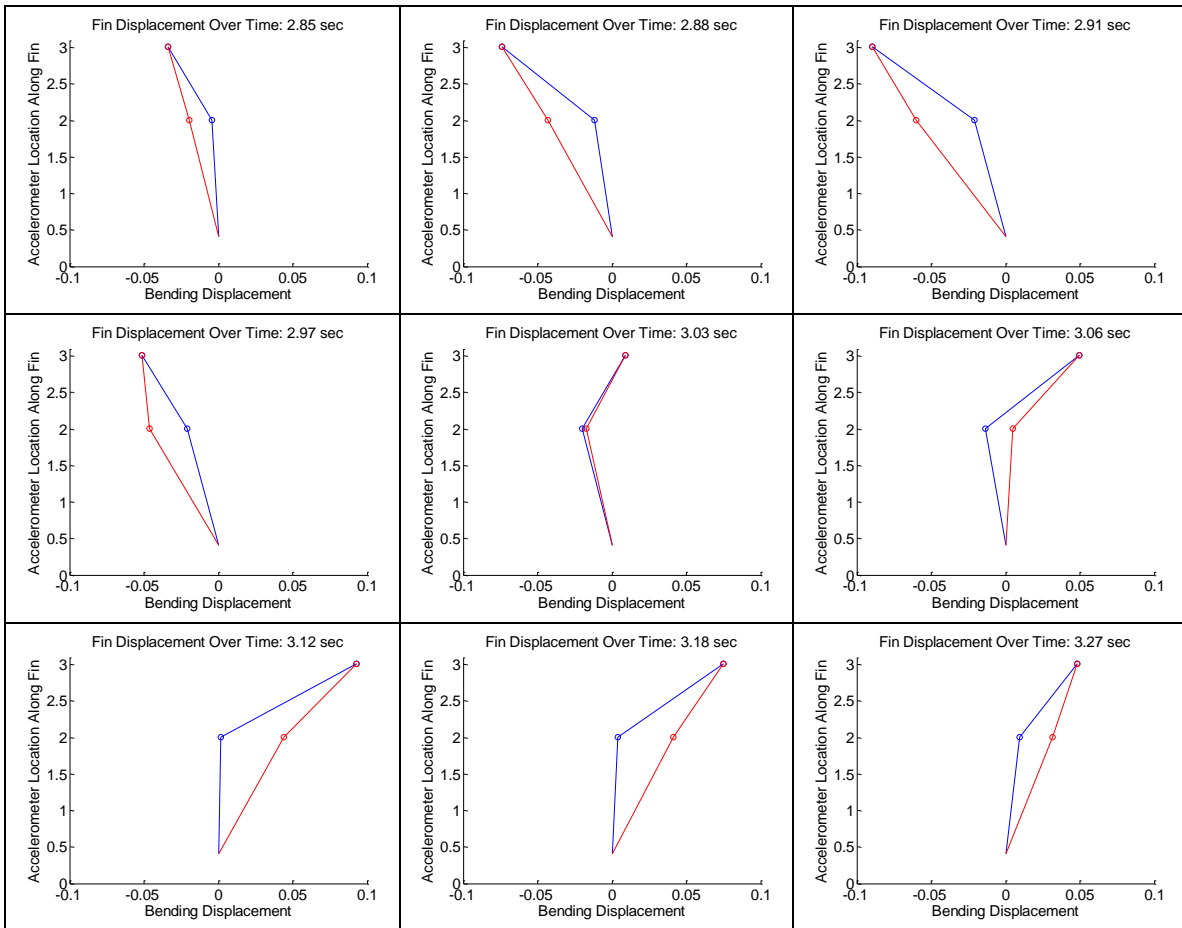


Figure 14. Fin Displacement Over Time.

Flutter movement is suggested beyond the quantitative analyses. Figure 15 shows that the fin moved during the experiment. Shown more clearly in Figure 16, the fin moved during the test runs, digging into the metal base plate. Figure 16 shows a zoomed-in look at the raised surface caused by the fin's movement.

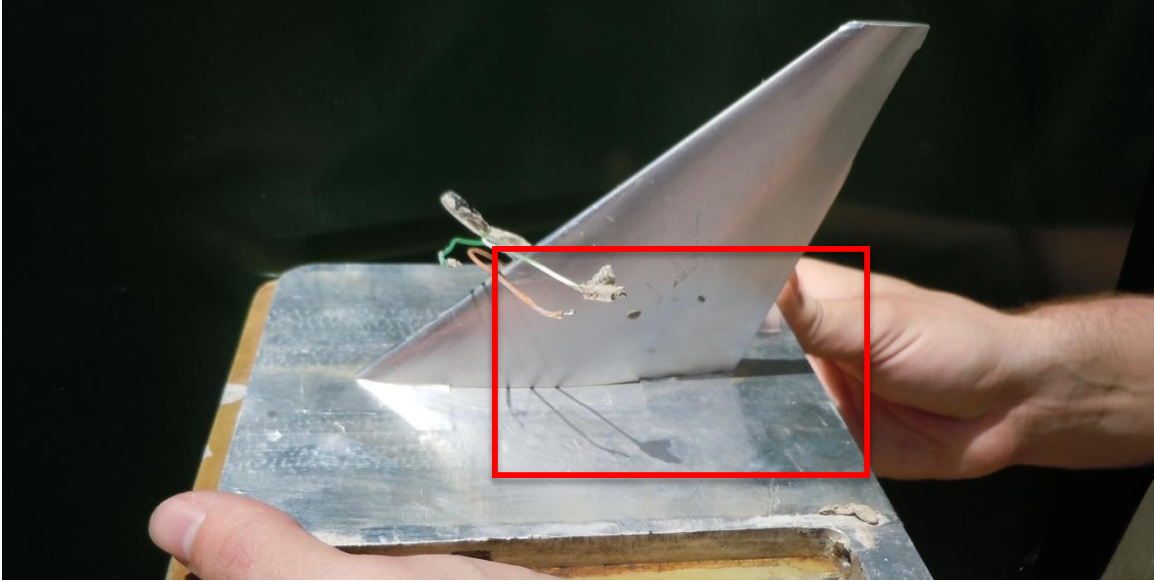


Figure 15. Image of the Fin After Run 2.



Figure 16. Highlighted portion of Figure 15.

VI. Future Work

This project is the ground work for future projects. It is the hope of this team that future students will continue the current progress. There are many areas in the project with room for improvement. The first improvement is utilizing better equipment to obtain more accurate results. Smaller sensors decrease their effect on the structural integrity and dynamics of the test wing. The team was unable to implement the

ADXL326 3-D accelerometer; however, future projects will hopefully devise a better soldering method to employ the 3-D sensor. The wing used in this experiment was overly customized to fit the dimensions of the wind tunnel, while being thick enough to house the accelerometers. Although the wing was shown to flutter in experimental NASA videos, it is the team's belief that the wing was too modified from the one shown in the video to achieve flutter in the experiment's conditions.

A second improvement is to securely mount the accelerometers into the test wing. The team relied on caulking putty to secure the accelerometers in the fin and provide a level surface with the wing. However, the high speeds of the test condition eventually stripped the putty away. Accelerometer three was completely lost and accelerometer four became partially detached. The use of epoxy to secure the accelerometers is suggested as a solution for future projects.

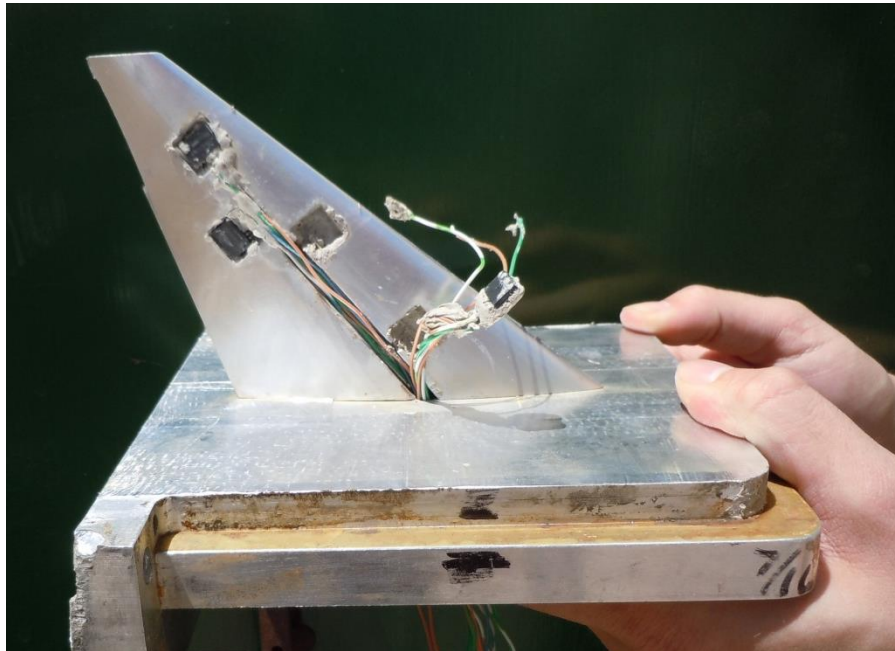


Figure 17. Detached Accelerometers. *In the final trial, two accelerometers detached from the wing and negated the data for the trial.*

Third, a better data acquisition setup is required to improve the accuracy of the experiment. Since the software model predicted displacement frequencies from 1000 to 5000 Hz, a high rate system is required. The current setup only achieved a data collection rate of 36 samples per second. Therefore, the current setup did not obtain enough data points to model the movement of the fin with a high resolution.

A final improvement is variability in the tunnel's speed. The theoretical calculations predicted airflow speeds that the supersonic wind tunnel could not achieve in its current state. Being able to modify the tunnel's configuration to achieve the required test airspeed will improve the results for future projects.

VII. Conclusion

The project yielded mixed results, with several areas for improvement for future projects. The data showed bending trends that at least agreed with the theoretical trends. Furthermore, the accelerometers located on the same chord line showed distinct movements, suggesting twist occurring in the wing. However, the increased bending deflections caused by the extra absorption of energy were only briefly exhibited, and dampened out unlike true flutter. These identifications are qualified within the limitations of the data acquisition setup. The DAQ system was incapable of capturing the displacements with a high enough resolution for confident results. Improving this system through smaller, higher performance accelerometers is the primary improvement for future projects. Adapting the wing model to fit the tunnel's dimensions and the larger accelerometers is the paramount reason for the lack of success in the project. Nonetheless, there is room for improvement to mitigate these issues for future projects to achieve more accurate results. Flutter remains an important element of a flight test envelope, requiring continued research.

References

¹Bae, J. S., and Lee, I., "Limit Cycle Oscillation of Missile Control Fin with Structural Non-Linearity," *Journal of Sound and Vibration*, January 2003.

²Martin, D. J., "Summary of Flutter Experiences as a Guide to the Preliminary Design of Lifting Surfaces on Missiles," *National Advisory Committee for Aeronautics*, February 1958.

³Megson, T. H. G., *Aircraft Structures for Engineering Students*, 4th ed., Elsevier Ltd., Oxford, 2007.